View metadata, citation and similar papers at core.ac.uk
brought to you by CORE
provided by Scholarship@Western

RESILIENT INFRASTRUCTURE
June 1–4, 2016
RESILIENT INFRASTRUCTURE LONDON 2016

BEHAVIOUR OF FRP-REINFORCED CFFT COLUMNS UNDER AXIAL COMPRESSION LOADING

Asmaa Abdeldaim Ahmed
M.Sc. Candidate, University of Sherbrooke, Canada

Radhouane Masmoudi, PE., PhD
Professor, University of Sherbrooke, Canada

ABSTRACT

This paper presents the test results of an experimental study aimed at investigating the axial behaviour of CFFT columns internally reinforced with steel and FRP bars. A total of eight reinforced concrete (RC) and concrete-filled FRP tube (CFFT) columns were constructed and tested until failure. All columns had 1900-mm in height and 213-mm in diameter. The test parameters were: (1) internal reinforcement type (steel, glass FRP (GFRP), or carbon FRP (CFRP) bars) and amount, (2) GFRP tube thicknesses, and (3) nature of axial loading type (i.e. monotonic and cyclic). The experimental results revealed that the CFFT columns reinforced with GFRP bars exhibited similar responses compared to their counterparts reinforced with steel bars with no significant difference in terms of ultimate axial strength and strain capacities. Providing the GFRP tubes of the CFFT columns significantly enhanced the strength and strain capacities and attributed to change the mode of failure from axially dominated material failure (for the control columns) to instability failure (for the CFFT columns). Furthermore, the envelop curve of the CFFT reinforced column tested under axial cyclic loading is almost identical to the axial stress-strain curve of the same specimen tested under axial monotonic loading. However, the ultimate axial and hoop rupture strain was slightly larger for the specimen subjected to axial cyclic loading. Finally, using FRP bars instead of conventional steel bars in the CFFT columns can provide a step forward to develop a promising totally corrosion-free new structural system.

Keywords: FRP; Concrete; CFFT; Tubes; Column; Axial.

1. INTRODUCTION

Fiber-reinforced polymer (FRP) composites have recently gained wide acceptance in the construction industry particularly of the aging infrastructures exposed to harsh environment conditions. An important application of FRP composites is as a confining material for concrete, both in the seismic retrofit of existing reinforced concrete (RC) columns and in the construction of concrete-filled FRP tubes (CFFTs) as earthquake-resistant columns in new construction. The promising concept of CFFT system, that may be further reinforced internally with steel or FRP bars, has raised great interest amongst researchers. The FRP tube acts as a stay-in-place structural formwork, a noncorrosive reinforcement for the concrete for flexure and shear using the multidirectional fiber orientation, provides confinement to the concrete in compression, and the contained concrete is protected from intrusion of moisture with corrosive agents that could otherwise deteriorate the concrete core (ACI 440. R-07-2007).

To date, most of the experimental investigations performed on FRP confined concrete columns have considered short, unreinforced, small-scale concrete cylinders, tested under concentric and monotonic axial loading (Mirmiran et al. 2001; Fam et al 2003; Lam and Teng 2009; Ozbakkaloglu et al 2013; Vincent and Ozbakkaloglu 2014). In contrast, only few studies have so far investigated the effects of the slenderness ratio and internal longitudinal reinforcement type (steel or FRP bars) on the behavior of FRP confined concrete long columns (Mirmiran et al 2001, Mohamed et al 2010, Fitzwilliam and Bisby 2010, and Masmoudi and Mohamed 2011). Yuan and Mirmiran (2001) carried out a comprehensive parametric study on the buckling of over 11 500 CFFT columns. They found that instability of CFFT columns might occur at a lower slenderness ratio than that of ordinary RC columns (without

FRP tubes); however, the ultimate capacity of the former might be higher than that of the latter. This attributed to the bilinear stress-strain behavior of the CFFT columns in which the buckling mode of failure initiated at the plastic branch of the curve, which was characterized by a lower Young's modulus. They also recommended that the current slenderness limit of 22 for steel-reinforced concrete columns bent in single curvature be reduced to 11 for CFFT columns. Masmodui and Mohamed (2011) conducted an experimental investigation on the axial behavior of CFFT columns internally reinforced with steel or carbon FRP (CFRP) bars with different slenderness ratios ranging from 4 to 20. The test results showed that the CFFT columns reinforced with CFRP bars behaved similar to that of CFFT columns reinforced with steel bars. The axial capacity of steel or CFRP-reinforced CFFT decreased as the slenderness ratios increased. This can draw the conclusion that the increase of the slenderness ratio of CFFT columns reinforced internally with steel or CFRP bars might be a critical factor that controls the mode of failure and might prevent such columns from attaining their ultimate load capacity.

FRP bars have emerged as a realistic and cost-effective solution to overcome such corrosion problems. Using FRP bars instead of conventional steel bars in the CFFT columns can provide a step forward to develop a promising totally corrosion-free new structural system. Nonetheless, the axial behavior of FRP bars as longitudinal reinforcement in compression members has been quite limited, especially for the CFFT columns. To the knowledge of the candidate, no investigations have addressed the behavior of FRP-reinforced CFFT columns under axial cyclic compression loading. To address such knowledge gaps and properly understanding the general behavior of FRP-reinforced CFFT columns under axial cyclic loading more experimental studies are needed. This paper presents the test results of an experimental study aimed at investigating the behavior of CFFT columns reinforced with longitudinal steel or FRP bars tested under axial compression loading. A total of eight RC and CFFT columns were constructed and tested until failure. All columns had 1900-mm in height and 213-mm in diameter. The effect of internal reinforcement type and amount, GFRP tube thicknesses, and natural of loading (i.e. monotonic and cyclic) were addressed.

2. EXPERIMENTAL WORK

2.1 Material Properties

All columns were constructed using a ready-mixed normal strength concrete (NSC) with an average compressive concrete strength of 44.1 MPa. The actual concrete compressive strength was determined from testing six concrete cylinders (150 × 300 mm) on the same day of testing the columns. Three types of longitudinal reinforcement were used to reinforce the control and CFFT columns: (1) deformed steel bars M15 (16 mm in diameter; 200 mm^2 in cross-sectional area); (2) GFRP bars No. 3 and No. 5 (9.5 mm and 15.9 mm in-diameter; 71 mm^2 and 199 mm^2 in cross-sectional area, respectively); and (3) CFRP bars No. 3 (9.5 mm-in diameter; 71 mm^2 in cross-sectional area). The mechanical properties of steel bars were determined from the standard test according to the ASTM A615/A615M-09 (2009) based on five representative specimens. Mild steel bar 3.4 mm in-diameter was served as transverse spiral reinforcement for the control specimens. The FRP bars had a sand-coated surface to improve the bond between the bars and surrounding concrete. The FRP bars tensile properties as provided by the manufacturer (Pultrall, Inc. 2009) are presented in Table 1.

Table 1: Tensile properties of the GFRP, CFRP, and steel bars

Reinforcement type	Nominal diameter (mm)	Nominal area (mm^2)	Tensile modulus of elasticity (GPa)	Yield strength (MPa)	Ultimate strength (MPa)	Ultimate strain (%)
GFRP	9.5	71	45.4	-	856	1.89
	15.9	199	48.2	-	751	1.60
CFRP	9.5	71	128	-	1431	1.20
Wire (mild steel)	3.4	9	200	675	850	0.30*
15M (deformed)	16	200	200	419	686	0.21*

* Yield strain

Two types of GFRP tubes (namely Type A and B), with an internal diameter of 213 mm and 2.9 and 6.4 mm wall thicknesses, respectively, were used as structural stay in-place formwork for the tested specimens (see Figure 1). The GFRP tubes were fabricated using filament-winding technique; E-glass fiber and Epoxy resin with different

fiber angles respect to the longitudinal axis of the tubes. The fiber orientations of the tubes were mainly in the hoop direction with no fibers in the longitudinal direction. Table 2 shows the dimensions and mechanical properties of FRP tubes. More details regarding the mechanical properties and standard tests of these tubes can be found elsewhere (Mohamed and Masmoudi 2010).

Figure 1: Filament wound GFRP tubes

Table 2: Dimension and mechanical properties of FRP tubes

Tube type	D (mm)	t_{frp} (mm)	No. of layers	Stacking sequence	f_{FRPU} (MPa)	ε_{FRPU} (%)	E_{FRPU} (MPa)	f_X (MPa)	ε_X (%)	E_X (MPa)
A	213	2.90	6	[60 º, 90 º, 60 º]	548	1.70	32260	55.2	0.62	8865
B	213	6.40	12	[±60 º, 90 º, ±60 º, 90 º]	510	1.69	30200	59.2	0.75	7897

D and t_{frp} are the internal diameter and thickness of the FRP tubes, respectively. f_{FRPU}, ε_{FRPU}, and E_{FRPU} are, respectively, the ultimate strength, ultimate tensile strain, and Young's modulus in the hoop direction; while f_X, ε_X, and E_x are the ultimate strength, ultimate tensile strain, and Young's modulus in the axial direction, respectively.

2.2 Test Specimens

A total of eight RC and CFFT circular columns were fabricated and tested under concentric axial monotonic or cyclic compression loading. Two RC control columns and six CFFT columns were internally reinforced with steel, Glass FRP (FRP) or CFRP bars. All columns had the same height (h=1900 mm) to diameter (D=213 mm) ratio of 9.0. The investigated test parameters were: (i) GFRP tubes thicknesses (2.9 and 6.4 mm); (ii) internal reinforcement type (steel; GFRP; or CFRP bars) and amount; and (iii) natural of loading (i.e. monotonic and cyclic). The control RC columns were reinforced longitudinally with reinforcement ratio (ρ_L) equal to (3.4%), one specimen reinforced with steel bars and the other specimen reinforced with GFRP bars. Steel spiral stirrups (pitch = 50.6 mm) were used as transverse reinforcement and designed to have approximately similar hoop stiffness as the GFRP tube (Type A). The CFFT columns were laterally confined with GFRP tubes (Type A or B). One specimen was internally reinforced with deformed steel bars (6 M15; ρ_L = 3.4%) and laterally confined with tube type (A). Four specimens were reinforced with 6 GFRP bars No. 3 or No. 5 (ρ_L = 1.2 and 3.4%, respectively) and laterally confined with tubes type (A and B). Besides, one specimen (A-$C_{(3.4)}$-C) was reinforced with longitudinal CFRP bars (6 No. 3; ρ_L = 1.2 %) and laterally confined with tube type (A) and was designed to have similar axial stiffness as in specimen (A-$G_{(3.4)}$-C). All specimens were tested under single complete unloading/reloading axial cyclic compression loading, except one specimen (B-$G_{(1.2)}$-M) which was tested under monotonic axial compression loading. Table 3 shows the test specimens' details.

The test specimens were labeled as follows: the first letter S, A, or B is defining "the type of lateral reinforcement: steel spiral stirrups, GFRP tube type (A), or tube type (B)" then followed by a letter S, G, or C indicating "the longitudinal reinforcement type: steel, GFRP, or CFRP bars", respectively. The number between brackets indicates "the longitudinal reinforcement ratio". The final letter refers to the natural of loading type "M for monotonic or C for complete unloading/reloading cyclic loading".

2.3 Instrumentations and Testing Procedures

Several strain gauges were mounted on the internal reinforcement bars prior the concrete casting and on concrete or GFRP tube surfaces before testing. Two strain gauges were bonded on two longitudinal bars at 180° degree apart at the mid-height of the column. Eight strain gauges were located at the column mid-height in both axial and lateral directions to measure the axial and lateral strains, respectively. Figure 2 (a & b) shows the strain gauges instrumentation on the reinforcing bars and GFRP tube surface. Two displacement transducers (DTs) were used to measure the axial deformation of the column over the full height as shown in Figure 3 (a). Additionally, two in-plane linear variable displacement transducers (LVDTs) were located at the mid-height to record the lateral displacements of each column. All columns were capped with a thin layer of the high strength sulphur to ensure uniform load distribution during testing. Before testing, both ends of the columns were further confined with bolted steel collars made from 10 mm thick steel plates in order to prevent premature failure at their ends. The specimens were loaded under axial compression loading using a 6000-kN capacity-testing machine. Loading and unloading in compression tests were achieved with load control at a rate approximately equal to 2.3 kN/s. During the test, load, axial and lateral displacements, and strain gauges were recorded automatically using a data acquisition system connected to the computer. Figure 3 shows the test setup: a) the test specimen inside the testing machine and b) data acquisition system.

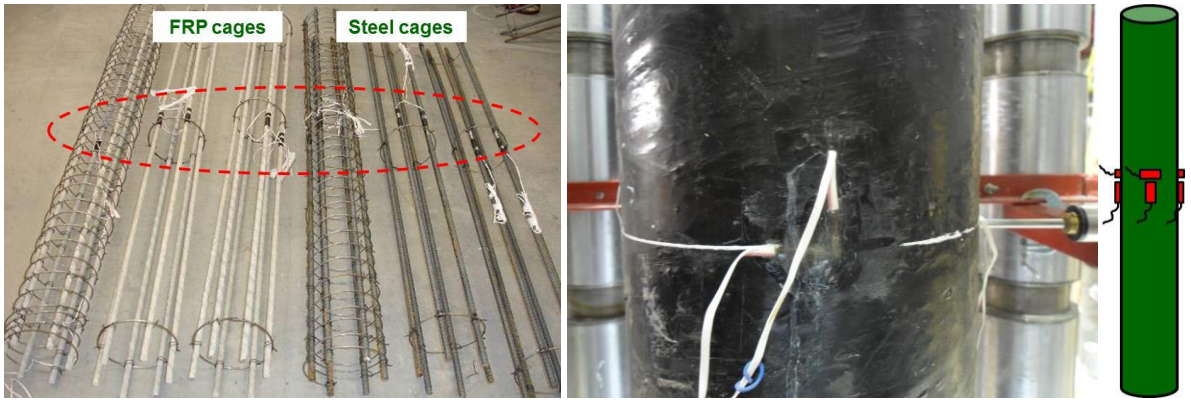

(a) (b)

Figure 2: Instrumentations: (a) reinforcement bars instrumentations (Mohamed 2010) and (b) vertical and horizontal strain gauges on the GFRP tube surface

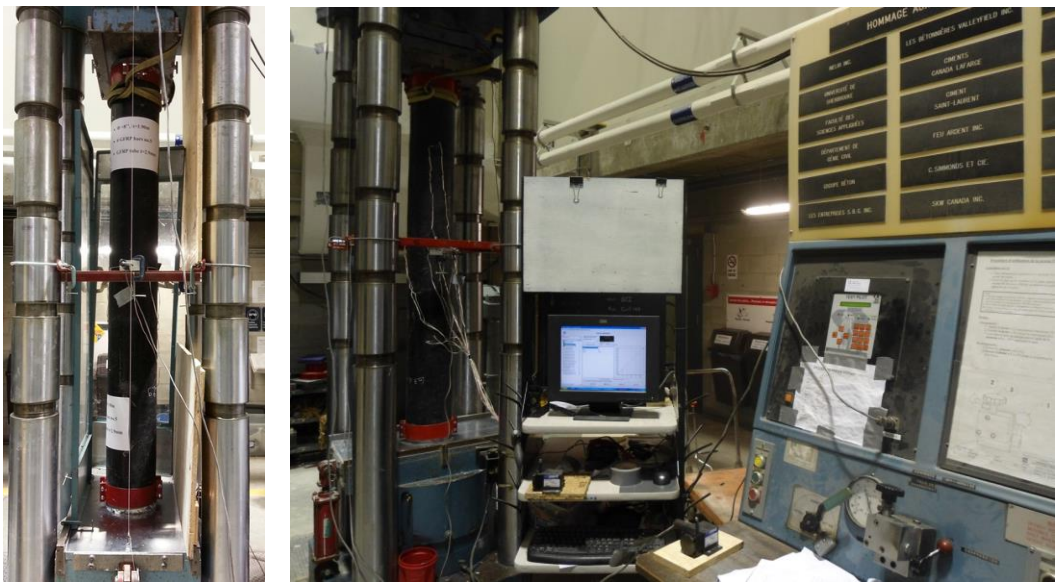

(a) (b)

Figure 3: Test setup: (a) test specimen inside the testing machine; (b) a data acquisition system

3. TEST RESULT AND DISCUSSION

3.1 Mode of Failure

Different failure modes were observed for the control and CFFT tested columns. For the control columns reinforced with steel or GFRP bars showed similar responses. The failure was typically initiated with vertical cracks started to appear at approximately 85% of their peak loads and followed by concrete dilation and lateral deformation of transverse and longitudinal reinforcement leading to concrete cover spalling. Thereafter, the concrete core crushed and spiral stirrups fractured after buckling of the longitudinal bars. Moreover, inclined diagonal shear surface was observed leading to a separation of the concrete core into two column parts causing a sudden drop after reaching the peak load. On the other hand, the CFFT columns showed substantially different failure mode compared to that occurred for the control columns. The GFRP tube provided significant confinement attributing to shift the failure mode from axially dominated material failure for control columns to instability failure for the CFFT columns. The instability was evident in a significant single curvature mode shape of the bent column. Despite, the specimens experienced much lateral deflections beyond the ultimate load, the deflected columns were still stable and carried more axial load. Loading the specimens continued until localized failure occurred near the mid height of the column. Finally, GFRP tube rupture, concrete crushing, and local buckling of steel bars or crushing of the FRP bars in the compression side of the CFFT columns were observed. This observation is in agreement with the previous research works conducted on slender FRP-confined columns (Mohamed et al 2010 and Fitzwilliam et al 2010). Figure 4 shows typical mode of failure for the tested columns. Table 3 summarizes the test results for all specimens.

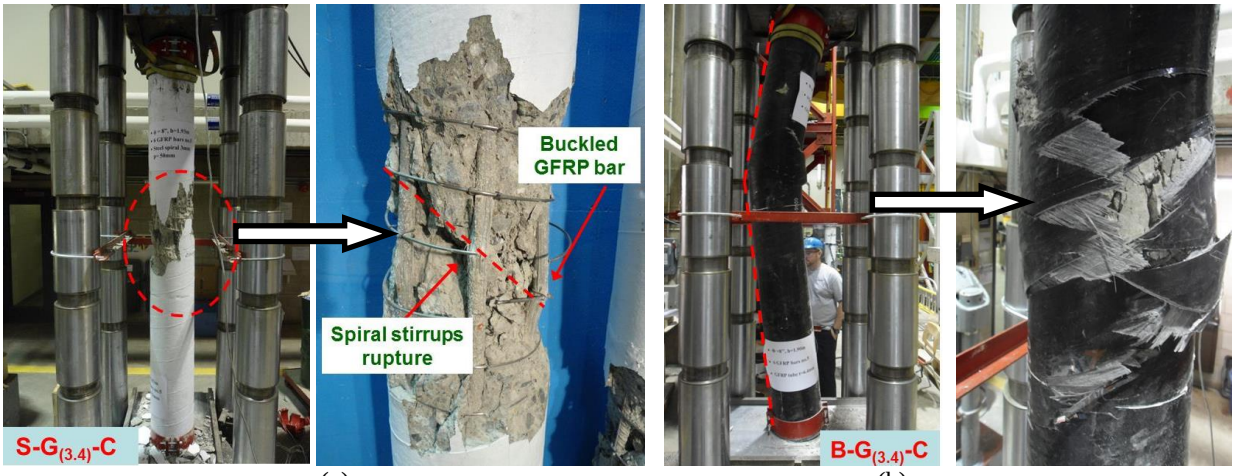

(a) (b)

Figure 4: Typical mode of failure for the tested columns: (a) GFRP-reinforced control specimen; (b) GFRP-reinforced CFFT column confined with tube (B)

3.2 Axial and Lateral Stress-Strain Responses

Figure 5 depicts the axial and lateral stress strain relationships for control and CFFT columns. Axial stress was obtained from dividing the axial load by the column cross-sectional. The axial and lateral stress-strain curves were plotted from the ultimate strain gauges bonded in the vertical and hoop directions at the mid-height of the column. The experimental results of the tested columns are shown in Table 3. In this Table 3, the experimental ultimate load (P_u), the confined concrete compressive strength (f_{cc}')-that is the maximum compressive strength at the ultimate load, the corresponding axial strain (ε_{cc}'), the unconfined concrete compressive strength (f_c') from cylinders and the corresponding axial strain of unconfined concrete (ε_{co}') are reported. As shown in Fig. 5 that the stress-strain diagrams for all columns exhibited almost similar initial stiffness with a relatively linear slope in the elastic range of the stress-strain curves, indicating that the elastic axial stiffness is not affected by confinement, regardless the investigated tested parameters. The stress-strain responses of the GFRP-reinforced control columns behaved similar to that of the steel-reinforced control column up to their peak load. However, the peak axial stress for steel-reinforced column was slightly higher than that of their counterpart reinforced with GFRP bars by 11% (on average).

The axial stress-strain curves for GFRP and steel reinforced CFFT columns showed similar shapes of the hysteresis loops for the unloading/reloading paths. However, the steel-reinforced CFFT column hysteresis loop starts to open after the yielding of steel bars. The unloading paths for the CFFT columns reinforced with steel or FRP bars exhibited non-linear behavior. The degree of the non-linearity increases as the unloading axial strain increases. The reloading paths can be resembled as straight lines. The envelop curves of the reinforced CFFT- columns, representing the upper boundary of the axial cyclic stress-strain responses, showed bilinear responses with a transition zone in the vicinity of the unconfined concrete (f_c') followed by nearly stabilization of the load carrying capacity as shown in specimens B-$G_{(3.4)}$-C and B-$G_{(1.2)}$-C). The initial slope was almost identical for all the specimens while the second slope is highly governed by GFRP tubes stiffness rather than the internal reinforcement type and amount, particularly in thicker tube thickness.

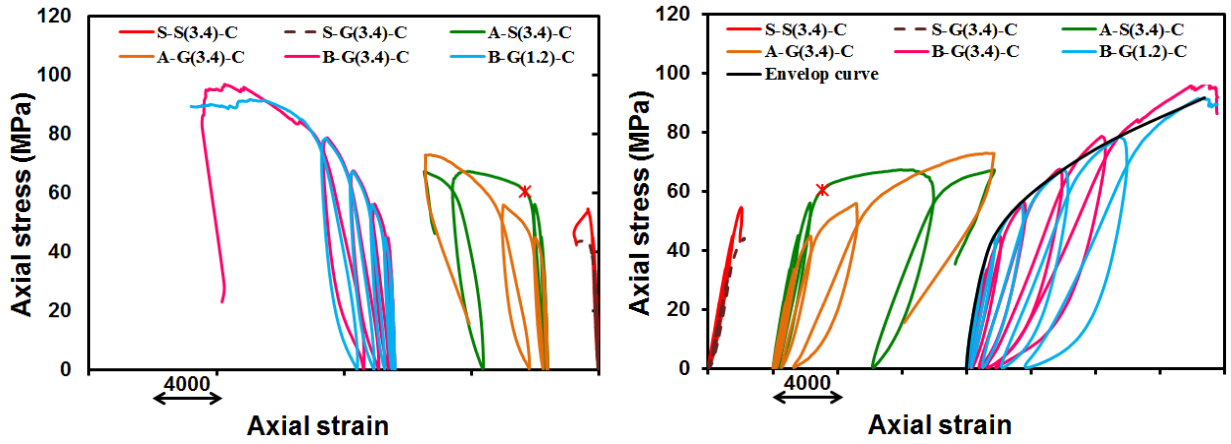

(a) Ultimate hoop strains (b) Ultimate axial strain

Figure 5: Axial cyclic stress-strain curves for control columns and reinforced-CFFT columns

Table 3: Specimen's details and test results

ID	Later reinforcement type	Longitudinal bars		P u (kN)	f'_{cc}[a] (MPa)	f'_{cc}/f'_c	ε_{cc} (με)	$\varepsilon_{cc}/\varepsilon_o$	$\varepsilon_{h,\ min.}$ (με)	$\varepsilon_{h,\ aver.}$ (με)	$\varepsilon_{h,\ max.}$ (με)
		Type	Area								
S-S(3.4)-C	ϕ3.4@50.6	Steel	6 M 15	1948	54.60	1.23	-2510	1.04	377	599	836
S-G(3.4)-C	ϕ3.4@50.6	GFRP	6 No. 5	1575	47.20	1.08	-2711	1.12	653	935	1144
A-S(3.4)-C	A	Steel	6 M 15	2402	67.38	1.53	-13749	3.83	2442	4697	9707
A-G(3.4)-C	A	GFRP	6 No. 5	2603	73.06	1.66	-13718	4.63	5172	8087	9610
B-G(3.4)-C	B	GFRP	6 No. 5	3455	96.97	2.20	-15578	5.49	4435	9745	15135
B-G(1.2)-C	B	GFRP	6 No. 3	3272	91.82	2.08	-15563	5.96	11456	13787	16113
B-G(1.2)-M	B	GFRP	6 No. 3	3068	86.09	1.95	-15514	5.15	3156	11356	16090
A-C(1.2)-C	A	CFRP	6 No. 3	2086	58.55	1.33	-15486	4.65	4190	8240	11913

* X-Y(aa)-Z*: X= lateral reinforcement type, where S=Steel spiral stirrups; A=GFRP tube type; and B= GFRP tube type B; Y=longitudinal reinforcement type, where S=steel bars; G= GFRP bars; and C=CFRP bars; aa=longitudinal reinforcement ratio; Z=loading type, where C=cyclic axial loading; and M=monotonic axial loading; [a] f_{cc}'=P_u/A_c

3.3 Stress-Strain Responses of Longitudinal Reinforcement

Figure 6 shows the axial stress-strain relationships for the longitudinal reinforcement of the tested specimens. As shown in Fig. 6a for the control columns reinforced with the GFRP and steel bars the average axial strains reached to 2495 and 2100 με, respectively. While the load carried by the reinforcement (computed by multiplying the area of the longitudinal reinforcement by the average axial strain and modulus of elasticity of the material) indicated that the GFRP and steel bars contributed to the ultimate load capacity of the columns by 10 and 15%, respectively. This confirms the integration of the GFRP bars used as the steel bars in compression for the tested columns (Mohamed et al 2014). For steel-reinforced CFFT column (A-$S_{(3.4)}$- C), the stress-strain curve for steel bars showed a linear response until yielding stress at a stain approximately equal to 2100 με (Fig. 6b). After yielding, the axial stress-steel strain increased progressively in the horizontal direction until failure. It was observed that the yield load occurred at load level 83% of the ultimate capacity. This indicated that the ultimate capacity did not show much enhancement

after yielding stage as a result of column instability occurred before initiation of the confinement lateral pressure. On the other hand, the GFRP-reinforced CFFT column initiated almost similarly response as steel-reinforced ones before steel yielding stage. Thereafter, the slope of axial stress-strain curve in the second region continued to increase slightly until failure. This can be attributed to the linear behavior of the FRP material. It showed be noted that both specimens (A-$S_{(3.4)}$-C and A-$G_{(3.4)}$-C) at the same longitudinal ratio (ρ=3.4%) achieved similar axial strength. This indicated that the contribution of the GFRP bars in the axial capacity of the CFFT column is comparable to that of the steel bars. Furthermore, increasing the longitudinal reinforcement ratio from 1.2 to 3.4% as in the tested specimens (B-$G_{(3.4)}$-C and B-$G_{(1.2)}$-C) demonstrated slightly increase in the axial load carrying capacity by only 5% (see Figure 6c).

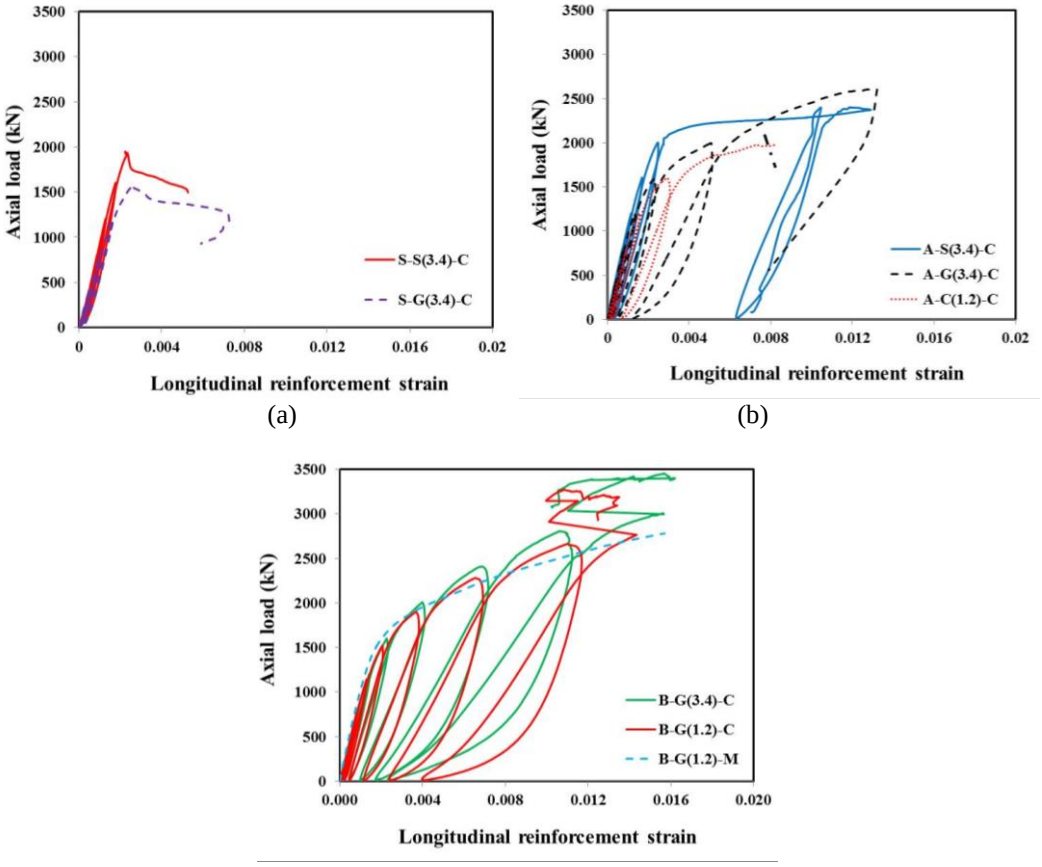

(a) (b)

(c)

Figure 6: Axial stress-strain relationships for longitudinal bars of the tested columns

3.4 GFRP Tube Thickness Effect on Confinement

Table 3 shows the strength and strain enhancement ratios (f'_{cc}/f'_c and $\varepsilon_{cc}/\varepsilon_{co}$). Table 3 indicates that the strength and strain enhancement ratios of the CFFT columns (A-$S_{(3.4)}$-C and A-$G_{(3.4)}$-C) were increased ranging from 1.3 to 1.5 and 3.7 to 4.4 times compared to their counterpart control specimens (S-$S_{(3.4)}$-C and S-$G_{(3.4)}$-C), respectively. As shown Figure 7 that providing the FRP tube as in tube A enhanced the strength and strain capacity by 52% and 470%, respectively, in comparison with their control specimens which were reinforced with steel spiral stirrups and designed to have similar lateral stiffness as in Tube A. This can be attributed to the continuity of the FRP tubes rather than the discontinuity of the steel stirrups, which reflects the superior confining behavior of the FRP tubes over the steel stirrups to increase not only the strength but also the ductility of the CFFT columns (Mohamed et al 2010). Increasing the GFRP tube thickness from 2.9 to 6.4 mm enhanced both the strength and strain ratios by 25% and 12%, respectively. This can be attributed to the enhancement of lateral confinement, as a result of increasing the stiffness of the tube, which increased the ultimate axial stress capacities and strain of the tested CFFT columns (see Figure 7).

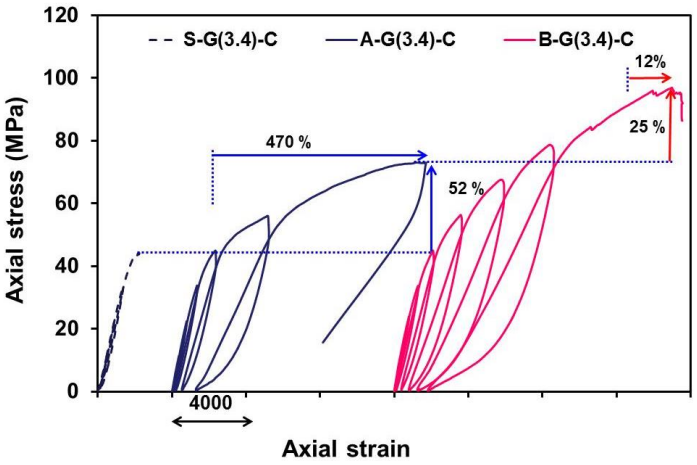

Figure 7: Axial cyclic stress-strain curves for specimens under different confinement type and level (S-$G_{(3.4)}$-C, A-$G_{(3.4)}$-C and B-$G_{(3.4)}$-C)

3.5 Effect of Loading Pattern

The envelop curves of the reinforced CFFT- columns, represent the upper boundary of the cyclic axial stress-strain responses.The responses in Figure 8 imply that the envelop curve of the GFRP-reinforced CFFT column (B-$G_{(1.2)}$-C) subjected to axial cyclic loading was almost identical to the axial stress-strain response of the monotonically loaded specimen (B-$G_{(1.2)}$-M). Generally, the ultimate axial strain of the axial cyclic loading specimen' was slightly higher than that of the specimen subjected to monotonic loading. This observation is consistent with the tests on FRP-confined concrete cylinders (Lam and Teng 2009; Sho et al. 2006; Ozbakkaloglu and Akin 2012). Furthermore, the average ultimate lateral strains of specimen (B-$G_{(1.2)}$-C) were 18% (on average) higher than the specimen (B-$G_{(1.2)}$-M), which is in agreement with pervious tests for axial cyclically loaded cylinders conducted by Lam and Teng 2009 and Theodoros 2001.

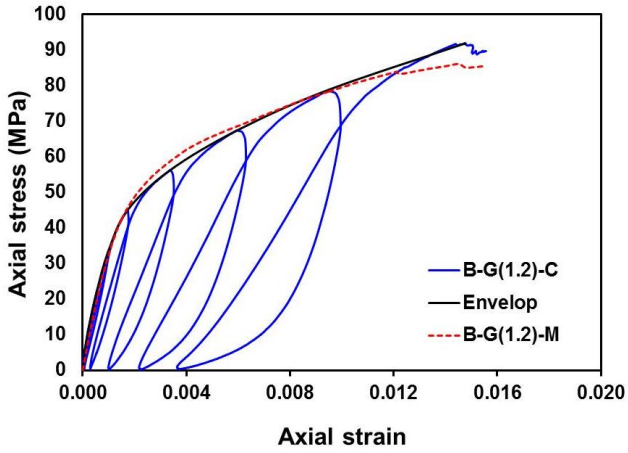

Figure 8: Stress-strain curves comparisons under axial cyclic and monotonic compression loading for specimens (B-$G_{(1.2)}$-C, and B-$G_{(1.2)}$-M)

CONCLUSIONS

This paper presented the results of an experimental study on the behavior of circular RC and CFFT columns internally reinforced with longitudinal steel or FRP bars tested under axial compression loading. The effect of internal reinforcement type and amount, GFRP tube thickness, and natural of loading type (monotonic or cyclic) were investigated. On the basis of the experimental test results and discussions of this paper, the following conclusions can be drawn:

1. The CFFT columns reinforced with GFRP bars exhibited similar responses compared to their counterparts reinforced with steel bars at the same longitudinal reinforcement amount. No significant difference was observed in terms of ultimate axial strength and strain capacities.
2. Increasing the thickness of the GFRP tubes significantly increased the ultimate axial and strain capacities of the CFFT reinforced tested columns.
3. The envelop curve of the CFFT reinforced column under axial cyclic loading is almost identical to the axial stress-strain curve of the same specimen under monotonic loading. However, the ultimate axial and hoop rupture strain was slightly larger for the specimen subjected to cyclic loading.
4. Using FRP bars instead of conventional steel bars in the CFFT columns can provide a step forward to develop a totally corrosion-free new structural system.

ACKNOWLEDGEMENTS

The reported research in this paper was partially sponsored by the Natural Sciences and Engineering Research Council of Canada (NSERC). The authors also acknowledge the contribution of the Canadian Foundation for Innovation (CFI) for the infrastructure used to conduct testing. Special thanks to the manufacturer (FRE Composites, QC, Canada) for providing FRP tubes.

REFERENCES

Abbasnia, R., Hosseinpour, F., Rostamian, M., Ziaadiny, H. 2013. Cyclic and monotonic behavior of FRP confined concrete rectangular prisms with different aspect ratios. *Construction and Building Materials*, (40):118–125.

ASTM A615/A615M-09, ASTM 2009. *Standard specification for deformed and plain carbon steel bars for concrete reinforcement*, West Conshohocken, Pa.

Fam, A., Greene, R. and Rizkalla, S. 2003. Field Applications of Concrete-Filled FRP Tubes for Marine Piles. *ACI Special Publication,* (*Field Application of FRP Reinforcement: Case Studies*) SP(215)9:161-180.

Fitzwilliam, J and Bisby, L. 2010. Slenderness Effects on Circular CFRP Confined Reinforced Concrete Columns. *Journal of Composites for Construction*, 14(3): 280-288.

Lam, L., and Teng, J. G. 2009. Stress-strain model for FRP-confined concrete under cyclic axial compression. *Eng. Struct.,* 31(2):308–321.

Masmoudi, R. and Mohamed, H. 2011. Axial behavior of slender-concrete-filled FRP tube columns reinforced with steel and carbon FRP bars. *10th International Symposium on Fiber-Reinforced Polymer Reinforcement for Concrete Structures*, Tampa, Florida, April 2011, ACI-SP-275.

Mirmiran, A.; Shahawy, M.; and Beitleman, T. 2001. Slenderness Limit for Hybrid FRP Concrete Columns. *Journal of Composites for Construction*, ASCE, 5(1): 26-34.

Mohamed, H., Abdel Baky, H. and Masmoudi, R., 2010, "Nonlinear stability analysis of CFFT columns: Experimental and Theoretical Investigations", ACI Structural Journal, V. 107, No. 6, pp. 699-708.

Mohamed, H.; Afifi, M.; and Benmokrane, B. 2014. Performance Evaluation of Concrete Columns Reinforced Longitudinally with FRP Bars and Confined with FRP Hoops and Spirals under Axial Load. *the Journal of Bridge Engineering*, © ASCE, ISSN /04014020(12) :1084-0702.

Ozbakkaloglu, T., and Akin, E. 2012. Behavior of FRP-confined normal- and high-strength concrete under cyclic axial compression. *J. Compos. Constr*, 2012(16):451-463.

Ozbakkaloglu, T, Lim, J, Vincent, T. 2013. FRP-confined concrete in circular sections: Review and assessment of stress–strain models. *Engineering Structures* 49:1068–1088.

Pultrall, Inc. 2007. V-ROD Composite Reinforcing Rods Technical Data Sheet. Thetford Mines, Canada, www.pultrall.com.

Shao, Y., Zhu, Z., and Mirmiran, A. 2006. Cyclic modeling of FRP confined concrete with improved ductility. *Cem. Concr. Compos*., 28(10): 959–968.

Theodoros R. 2001. Experimental investigation of concrete cylinders confined by carbon FRP sheets, under monotonic and cyclic axial compression load. Research Report. Publication 01: 2. *Division of Building Technology*, Chalmers University of Technology.

Vincent, T. and Ozbakkaloglu T. 2014. Influence of Slenderness on Stress-Strain Behavior of Concrete-Filled FRP Tubes: Experimental Study. *Journal of Composites for Construction*, © *ASCE*, ISSN 1090-0268/04014029(13).

Wang, Z; Wang, D.; Smith, S., Lu, D., 2012. CFRP-Confined Square RC Columns. II: Experimental Investigation. *the Journal of Composites for Construction*, 16(2). ©ASCE, ISSN 1090-0268/2012/2- 150–160.

Yuan, W., and Mirmiran, A., 2001. Buckling Analysis of Concrete- Filled FRP Tubes. *International Journal of Structural Stability and Dynamics*, 1(3):367-383.